

Parametrization of the Magnetic Behavior of the Triangular Spin Ladder Chains Organically Templated: $(C_2N_2H_{10})[M(HPO_3)F_3]$ ($M^{III} = Fe, Cr,$ and V). Crystal Structure and Thermal and Spectroscopic Properties of the Iron(III) Phase

Sergio Fernández-Armas,[†] José L. Mesa,^{*†} José L. Pizarro,[‡] Juan Modesto Clemente-Juan,[§] Eugenio Coronado,[§] María I. Arriortua,[‡] and Teófilo Rojo^{*†}

Departamento de Química Inorgánica and Departamento de Mineralogía y Petrología, Facultad de Ciencia y Tecnología, Universidad del País Vasco, Apartado 644, E-48080 Bilbao, Spain, and Instituto de Ciencia Molecular, Universidad de Valencia, 46100 Burjassot-Valencia, Spain

Received October 19, 2005

A new iron(III) phosphite templated by ethylenediamine has been synthesized using solvothermal conditions under autogenous pressure. The $(C_2N_2H_{10})[Fe(HPO_3)F_3]$ compound has been characterized by single-crystal X-ray diffraction data and spectroscopic and magnetic techniques. The crystal structure is formed by chains extended along the c axis and surrounded by ethylenediammonium cations. A study by diffuse-reflectance spectroscopy has been performed, and the calculated Dq , B , and C parameters for the Fe^{III} cations are 1030, 720, and 3080 cm^{-1} , respectively. The Mössbauer spectrum at room temperature is characteristic of Fe^{III} ions. The electron spin resonance (ESR) spectra carried out at different temperatures show isotropic signals with a g value of 2.00(1). The thermal evolution of the intensity of the ESR signals indicates the existence of antiferromagnetic interactions for the Fe^{III} phase. The magnetic susceptibility data of the Cr^{III} and V^{III} compounds show antiferromagnetic couplings. The J -exchange parameters of the Fe^{III} and Cr^{III} compounds have been calculated by using a model for a triangular spin ladder chain. The values are $J_1 = -1.63(1)\text{ K}$ and $J_2 = -0.87(2)\text{ K}$ with $g = 2.02$ for the Fe^{III} phase and $J_1 = -0.56(2)\text{ K}$ and $J_2 = -0.40(2)\text{ K}$ with $g = 1.99$ for the Cr^{III} compound. In the case of the V^{III} phase, the fit has been performed considering a linear chain with the magnetic parameters $D = 2.5\text{ cm}^{-1}$ and $J = -1.15(1)\text{ K}$.

Introduction

Open-framework materials are of great interest from both the industrial and academic points of view because of their catalytic, adsorbent, and ion-exchange properties.¹ While the large voids, chemical stability, and size-discriminatory absorptive behavior of zeolites render them very useful, open-framework solids containing transition elements could provide novel properties including catalytic, electronic, and magnetic properties inaccessible in main-group systems. It

has been recently shown that the incorporation of H-bonded organic molecules, especially diammonium cations, via solvothermal synthesis is a very general method for the preparation of a large variety of novel organically templated materials such as phosphates, phosphonates, and oxides with a large variety of transition-metal ions.² This synthetic procedure based on the use of organic diamines as structure-direct agents under mild solvothermal conditions (10–20 bar, 170 °C) leads to one-, two-, or three-dimensional open frameworks,^{1a} in which the templating molecule establishes H bonds and ionic interactions with the inorganic skeleton.

* To whom correspondence should be addressed. E-mail: joseluis.mesa@ehu.es (J.L.M.); teo.rojo@ehu.es (T.R.). Phone: 34-946015523 (J.L.M.); 34-946012458 (T.R.). Fax: 34-944648500.

[†] Departamento de Química Inorgánica, Universidad del País Vasco.

[‡] Departamento de Mineralogía y Petrología, Universidad del País Vasco.

[§] Universidad de Valencia.

(1) (a) Cheetham, A. K.; Ferey, G.; Loiseau, T. *Angew. Chem., Int. Ed.* **1999**, *38*, 3268. (b) Davis, M. E.; Lobo, R. F. *Chem. Mater.* **1992**, *4*, 756. Breck, D. W. *Zeolite Molecule Sieves: Structure, Chemistry and Use*; John Wiley & Sons: New York, 1974. (c) Venuto, P. B. *Microporous Mater.* **1994**, *2*, 297.

(2) (a) Haushalter, R.; Mundi, L. *Chem. Mater.* **1992**, *4*, 31. (b) Soghomonian, V.; Chen, Q.; Haushalter, R.; Zubieta, J. *Chem. Mater.* **1993**, *5*, 1690. (c) Kahn, M.; Lee, Y.; O'Connor, C.; Haushalter, R.; Zubieta, J. *J. Am. Chem. Soc.* **1994**, *116*, 4525. (d) Zapf, P.; Rose, D.; Haushalter, R.; Zubieta, J. *J. Solid State Chem.* **1996**, *125*, 182. (e) DeBord, J.; Haushalter, R.; Zubieta, J. *J. Solid State Chem.* **1996**, *125*, 270. (f) Dhingra, S.; Haushalter, R. *J. Chem. Soc., Chem. Commun.* **1993**, *21*, 1665. (g) Zhang, Y.; O'Connor, C.; Clearfield, A.; Haushalter, R. *Chem. Mater.* **1996**, *8*, 595.

Although designing phases similar to aluminosilicate zeolitic structures has been the subject of main interest in the study of these materials, the discovery of new compounds with novel structural features has also assumed an important role.^{1a,3} With the development of zeolite aluminosilicate and metal phosphate, which constitute the best-known classes of open-framework structures, a thorough study was made in the synthesis of open-framework phosphates.^{4a,b} Among the organically templated open-framework materials, metal phosphates occupy a first position. Several works dealing with organically templated iron phosphates have evidenced a rich structural chemistry in this system.^{4c,f}

The possibilities of incorporating P^{III} as pseudopyramidal $(HPO_3)^{2-}$ hydrogen phosphite into extended structures templated by inorganic alkaline-earth cations were explored a few years ago.⁵ However, the organically templated phosphites with metallic transition elements have not been extensively studied. Compounds with the V^{IV} , Co^{II} , Fe^{II} , Mn^{II} , Fe^{III} , V^{III} , and Cr^{III} cations are now known.⁶ To complete the knowledge about these types of materials incorporating metallic magnetic cations belonging to the first series of transition elements, we have synthesized the phosphite of formula $(C_2N_2H_{10})[Fe(HPO_3)F_3]$. The crystal structure of this compound and the spectroscopic and magnetic properties are also reported. This organically templated material is a new member of the family of compounds $(C_2N_2H_{10})-$

$[M(HPO_3)F_3]$,^{6g} where M is a trivalent metallic cation belonging to the 3d series of transition elements. A magnetic model for the analysis of the magnetic data of the $(C_2N_2H_{10})-[M(HPO_3)F_3]$ ($M^{III} = Fe, Cr, \text{ and } V$) family of compounds has been elaborated.

Experimental Section

Synthesis and Characterization. The $(C_2N_2H_{10})[Fe(HPO_3)F_3]$ phase has been synthesized using mild solvothermal conditions under autogenous pressure. The starting reagents were $FeCl_3 \cdot 6H_2O$ (1.50 mmol), H_3PO_3 (15 mmol), HF (50 mmol), and ethylenediamine (23 mmol) in a mixture of water/ethanol with a 1.7:1 ratio. This reaction mixture was stirred until homogeneity. After that, it was placed in a poly(tetrafluoroethylene)-lined stainless steel pressure vessel (fill factor 75%) and heated to 170 °C for 5 days, followed by slow cooling to room temperature. The pH of the mixture did not show any appreciable change during the solvothermal reaction and remained at approximately 5.0. The compound was obtained as single crystals. The yield was approximately 78%. The percentage of the elements in the products was calculated by inductively coupled plasma atomic emission spectroscopy and C, H, N elemental analysis. The F content was determined by using a selective electrode. Anal. Calcd for $(C_2N_2H_{10})[Fe(HPO_3)F_3]$: Fe, 21.1; P, 12.2; C, 9.4; H, 4.4; N, 11.0; F, 22.4. Found: Fe, 20.8; P, 11.9; C, 9.1; H, 4.2; N, 10.8; F, 22.1. The density measured by flotation in a mixture of $CHCl_3/CHBr_3$ is 2.149(7) $g\ cm^{-3}$.

The thermogravimetric analysis (TGA) study was performed under synthetic air in a SDC simultaneous differential scanning calorimetry (DSC)–TGA TA instrument. Crucibles containing approximately 20 mg of sample were heated at 5 °C min^{-1} in the temperature range 30–800 °C. The decomposition curve of $(C_2N_2H_{10})[Fe(HPO_3)F_3]$ shows an exothermic mass loss between room temperature and 310 °C of approximately 24.4%, which is assigned to the calcinations of the ethylenediammonium cation (23.6%). An additional exothermic weight loss was observed in the 320–500 °C range. This loss has been attributed to the elimination of the fluoride anion and the oxidation process of the phosphite oxoanion to phosphate groups. Above 500 °C, no mass loss was observed. The inorganic residue obtained at 800 °C was identified by X-ray diffraction powder as formed by the trigonal $Fe(PO_4)$ [$P3_121$, $a = 5.03(1)$ Å, and $c = 11.23(1)$ Å]^{7a} and $Fe_3O_3(PO_4)$ [$R3m$, $a = 8.01(1)$ Å, and $c = 6.86(1)$ Å] phases.^{7b}

The thermal behavior of the $(C_2N_2H_{10})[Fe(HPO_3)F_3]$ compound was also studied by using time-resolved X-ray thermodiffraction in synthetic air. A Philips X'PERT automatic diffractometer (Cu $K\alpha$ radiation) equipped with a variable-temperature stage (Paar Physica TCU2000) with a Pt sample holder was used in the experiment. The powder patterns were recorded in 2θ steps of 0.02° in the range $5 \leq 2\theta \leq 45^\circ$, counting for 1 s per step and increasing the temperature at 5 °C min^{-1} for room temperature up to 800 °C. $(C_2N_2H_{10})[Fe(HPO_3)F_3]$ is stable up to 240 °C, and the intensity of the monitored (200) maximum at $2\theta = 13.7^\circ$ remains practically unchanged (Figure 1). Above this temperature, a rapid decrease of the crystallinity of the compound takes place and it finally becomes amorphous. Thus, in the 240–510 °C range, no peaks were observed in the X-ray patterns. These results indicate the existence of a collapse of the crystal structure of this compound with the loss of the ethylenediammonium cation. In the 510–600 °C range, the maxima corresponding to the orthorhombic $Fe(PO_4)$ are

- (3) (a) Choudhury, A.; Natarajan, S.; Rao, C. N. R. *J. Solid State Chem.* **1999**, *146*, 538. (b) Cavelllec, M. R.; Riou, D.; Ferey, G. *Inorg. Chim. Acta* **1999**, *291*, 317.
- (4) (a) Cao, G.; Hong, H.; Mallouk, T. E. *Acc. Chem. Res.* **1992**, *25*, 420. (b) Bibby, D. M.; Dale, M. P. *Nature* **1985**, *317*, 157. (c) Lii, K.-H.; Huang, Y.-F.; Zima, V.; Huang, C.-Y.; Lin, H.-M.; Jiang, Y.-C.; Liao, F.-L.; Wang, S.-L. *Chem. Mater.* **1998**, *10*, 2599. (d) Cavelllec, M.; Riou, D.; Greneche, J. M.; Ferey, G. *Inorg. Chem.* **1997**, *36*, 2181. (e) DeBord, J. R. D.; Reiff, W. M.; Warren, C. J.; Haushalter, R.; Zubieta, J. *Chem. Mater.* **1997**, *9*, 1994. (f) Lii, K.-H.; Huang, Y. F. *J. Chem. Soc., Chem. Commun.* **1997**, 1311.
- (5) (a) Shieh, M.; Martin, K. J.; Squattrito, P. J.; Clearfield, A. *Inorg. Chem.* **1990**, *29*, 958. (b) Sapiña, F.; Gomez, P.; Marcos, M. D.; Amoros, P.; Ibáñez, R.; Beltrán, D. *Eur. J. Solid State Inorg. Chem.* **1989**, *26*, 603. (c) Marcos, M. D.; Amoros, P.; Beltrán, A.; Martínez, R.; Atfield, J. P. *Chem. Mater.* **1993**, *5*, 121. (d) Atfield, M. P.; Morris, R. E.; Cheetham, A. K. *Acta Crystallogr.* **1994**, *C50*, 981. (e) Marcos, M. D.; Amoros, P.; Le Bail, A. *J. Solid State Chem.* **1993**, *107*, 250. (f) Harrison, W. T. A.; Phillips, M. L.; Chavez, V.; Nenoff, T. M. *J. Mater. Chem.* **1999**, *9*, 3087. (g) Rodgers, J. A.; Harrison, W. T. A. *Chem. Commun.* **2000**, 2385. (h) Harrison, W. T. A.; Phillips, M. L.; Stanchfield, J.; Nenoff, T. M. *Inorg. Chem.* **2001**, *40*, 895. (i) Johnstone, J. A.; Harrison, W. T. A. *Inorg. Chem.* **2004**, *43* (15), 4567. (j) Kirkpatrick, A.; Harrison, W. T. A. *Solid State Sci.* **2004**, *6* (6), 593. (k) Gordon, L. E.; Harrison, W. T. A. *Inorg. Chem.* **2004**, *43* (6), 1808.
- (6) (a) Bonavia, G.; DeBord, J.; Haushalter, R. C.; Rose, D.; Zubieta, J. *Chem. Mater.* **1995**, *7*, 1995. (b) Fernandez, S.; Mesa, J. L.; Pizarro, J. L.; Lezama, L.; Arriortua, M. I.; Olazcuaga, R.; Rojo, T. *Chem. Mater.* **2000**, *12*, 2092. (c) Fernandez, S.; Pizarro, J. L.; Mesa, J. L.; Lezama, L.; Arriortua, M. I.; Olazcuaga, R.; Rojo, T. *Inorg. Chem.* **2001**, *40*, 3476. (d) Fernandez, S.; Pizarro, J. L.; Mesa, J. L.; Lezama, L.; Arriortua, M. I.; Rojo, T. *Int. J. Inorg. Mater.* **2001**, *3*, 331. (e) Fernandez, S.; Mesa, J. L.; Pizarro, J. L.; Lezama, L.; Arriortua, M. I.; Rojo, T. *Chem. Mater.* **2002**, *14*, 2300. (f) Fernández, S.; Mesa, J. L.; Pizarro, J. L.; Lezama, L.; Arriortua, M. I.; Rojo, T. *Angew. Chem., Int. Ed.* **2002**, *41*, 3683. (g) Fernandez, S.; Mesa, J. L.; Pizarro, J. L.; Lezama, L.; Arriortua, M. I.; Rojo, T. *Chem. Mater.* **2003**, *15*, 1204. (h) Fernández-Armaz, S.; Mesa, J. L.; Pizarro, J. L.; Garitaonandia, J. S.; Arriortua, M. I.; Rojo, T. *Angew. Chem., Int. Ed.* **2004**, *43* (8), 977. (i) Bazan, B.; Mesa, J. L.; Pizarro, J. L.; Peña, A.; Arriortua, M. I.; Rojo, T. *Z. Anorg. Allg. Chem.* **2005**, *631*, 2026. (j) Fernández-Armaz, S.; Mesa, J. L.; Pizarro, J. L.; Chung, U.-C.; Arriortua, M. I.; Rojo, T. *J. Solid State Chem.* **2005**, *178*, 3554.

(7) Powder Diffraction File—Inorganic and Organic; ICDD File Nos. (a) 84-876, (b) 76-1761, and (c) 30-659; International Centre for Diffraction Data: Newton Square, PA, 1995.

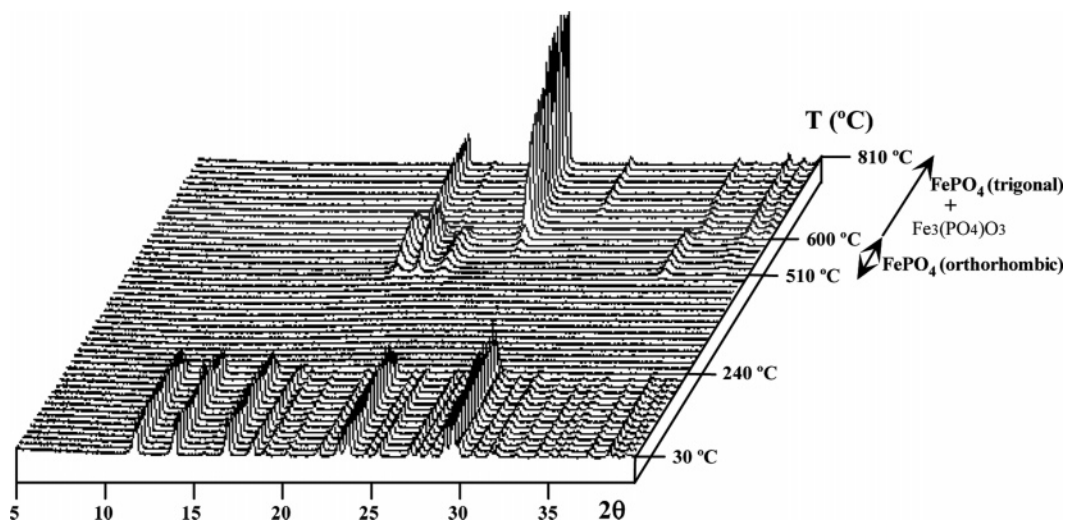


Figure 1. Thermodiffractogram of $(\text{C}_2\text{N}_2\text{H}_{10})[\text{Fe}(\text{HPO}_3)\text{F}_3]$.

Table 1. Crystal Data, Details of Data Collection, and Structural Refinement for $(\text{C}_2\text{N}_2\text{H}_{10})[\text{Fe}(\text{HPO}_3)\text{F}_3]$

| | |
|---|---|
| formula | $\text{C}_2\text{H}_{11}\text{F}_3\text{FeN}_2\text{O}_3\text{P}$ |
| molecular weight (g mol ⁻¹) | 254.95 |
| cryst syst | orthorhombic |
| space group | $P2_12_12_1$ (No. 19) |
| a , Å | 12.906(4) |
| b , Å | 9.528(2) |
| c , Å | 6.438(2) |
| V , Å ³ | 791.7(4) |
| Z | 4 |
| ρ_{calc} , g cm ⁻³ | 2.139 |
| $F(000)$ | 516 |
| T , K | 293 |
| radiation, $\lambda(\text{Mo K}\alpha)$, Å | 0.710 73 |
| $\mu(\text{Mo K}\alpha)$, mm ⁻¹ | 2.133 |
| limiting indices | $-15 < h < 15, -11 < k < 11, -7 < l < 7$ |
| $R [I > 2\sigma(I)]$ | $R1 = 0.0361, wR2 = 0.0624^a$ |
| R [all data] | $R1 = 0.0686, wR2 = 0.0682^a$ |
| GOF | 0.821 |
| Flack parameter | 0.05(4) |

^a $R1 = [\sum(|F_o| - |F_c|)] / \sum|F_o|$; $wR2 = [\sum[w(|F_o|^2 - |F_c|^2)^2] / \sum[w|F_o|^2]^2]^{1/2}$; $w = 1/[\sigma^2|F_o|^2 + (x p)^2]$, where $p = [|F_o|^2 + 2|F_c|^2] / 3$ and $x = 0.0275$.

observed in the thermodiffractograms [$Cmcm$, $a = 5.23(1)$ Å, $b = 7.77(1)$ Å, and $c = 6.32(1)$ Å].^{7c} This phase was not observed in the TGA study. At 600 °C, peaks of the trigonal polymorph $\text{Fe}(\text{PO}_4)^{7a}$ appear together with those corresponding to the trigonal $\text{Fe}_3(\text{PO}_4)\text{O}_3$ phase [$R3m$, $a = 8.01(1)$ Å, and $c = 6.86(1)$ Å],^{7b} as was observed in the inorganic residue obtained from the TGA study. Above 600 °C and up to 800 °C, no change was detected in the X-ray powder patterns from the thermodiffractograms.

Single-Crystal X-ray Diffraction. Prismatic single crystals of $(\text{C}_2\text{N}_2\text{H}_{10})[\text{Fe}(\text{HPO}_3)\text{F}_3]$ with dimensions $0.06 \times 0.06 \times 0.12$ mm and relatively good quality were carefully selected under a polarizing microscope and mounted on a glass fiber. Diffraction data were collected at room temperature on a STOE IPDS (imaging plate diffraction system), using graphite-monochromated Mo K α radiation. Details of the crystal data, intensity collection, and some features of the structural refinement are reported in Table 1.

A total of 5059 reflections were measured in the range $3.54 \leq \theta \leq 26.01^\circ$, which were considered to be 1529 independent ($R_{\text{int}} = 0.0631$) and 1017 observed, applying the criterion $I > 2\sigma$. The software of the STOE IPDS diffractometer⁸ was used to perform

the corrections for Lorentz and polarization effects. The absorption corrections were carried out by using the XRED program,⁹ taking into account the shape and size of the crystal. The structure was solved by direct methods (SHELXS 97 program)¹⁰ and refined by full-matrix least squares based on F^2 , using the SHELXL 97 program.¹¹ The scattering factors were taken from ref 12. Anisotropic thermal parameters were assigned to the non-H atoms. The coordinates of the H atoms of the phosphite anions were obtained from the difference Fourier maps, and those of the ethylenediammonium cation were geometrically placed. Final R factors $R1 = 0.069$ (all data) [$wR2 = 0.068$]. Maximum and minimum peaks in the final difference synthesis were 0.432 and -0.472 e Å⁻³, respectively. The GOF on F^2 was 0.821. A simulation based on the single-crystal structure was in excellent agreement with the X-ray powder data, indicating the presence of a pure phase with high crystallinity. The structure factor parameters have been deposited at the Cambridge Crystallographic Data Centre (CCDC 224863). All drawings were made using the ATOMS program.¹³ Selected bond distances and angles are given in Table 2.

Physicochemical Characterization Techniques. The IR spectrum (KBr pellets) was obtained with a Nicolet FT-IR 740 spectrophotometer in the 400–4000-cm⁻¹ range. The Raman spectrum was recorded in the 200–3000-cm⁻¹ range, with a Nicolet 950FT spectrophotometer equipped with a Nd laser emitting at 1064 nm. A diffuse-reflectance spectrum was registered at room temperature on a Cary 2415 spectrometer in the 210–2000-nm range. Mössbauer measurements were recorded at room temperature in the transmission geometry using a conventional constant-acceleration spectrometer with a ⁵⁷CoRh source. A Bruker ESP 300 spectrometer was used to record the ESR polycrystalline spectra performed at X band from room temperature to 5.0 K. The temperature was stabilized by an Oxford Instruments (ITC 4) regulator. The magnetic field was measured with a Bruker BNM 200 gaussmeter, and the frequency inside the cavity was determined using a Hewlett-Packard 5253B microwave frequency counter.

(9) XRED; Stoe & Cie GmbH: Darmstadt, Germany, 1998.

(10) Sheldrick, G. M. SHELXS 97: Program for the Solution of Crystal Structures; University of Göttingen: Göttingen, Germany, 1997.

(11) Sheldrick, G. M. SHELXL 97: Program for the Refinement of Crystal Structures; University of Göttingen: Göttingen, Germany, 1997.

(12) International Tables for X-ray Crystallography; Kynoch Press: Birmingham, U.K., 1974; Vol. 4, p 99.

(13) Dowty, E. ATOMS: A Computer Program for Displaying Atomic Structures; Shape Software (521 Hidden Valley Road): Kingsport, TN, 1993.

(8) Stoe IPDS Software, version 2.87; Stoe & Cie: Darmstadt, Germany, 1998.

Table 2. Selected Bond Distances (Å) and Angles (deg) for $(C_2N_2H_{10})[Fe(HPO_3)F_3]$ (Estimated Standard Deviation in Parentheses)^a

| Bond Distances (Å) | | | |
|--|----------|----------------------------|----------|
| FeO ₆ Octahedron | | | |
| Fe–F(1) | 1.907(3) | Fe–O(2) | 1.979(3) |
| Fe–F(3) | 1.957(3) | Fe–F(2) | 1.989(3) |
| Fe–O(3) | 1.975(5) | Fe–O(1) | 2.005(4) |
| HPO ₃ Tetrahedron | | | |
| P–O(2) ⁱ | 1.498(3) | P–O(3) ⁱⁱ | 1.523(5) |
| P–O(1) | 1.509(5) | P–H(1) | 1.39(2) |
| (H ₃ N–CH ₂ –CH ₂ –NH ₃) ⁺ /Ethylenediammonium | | | |
| N(1)–C(1) | 1.475(7) | N(2)–C(2) | 1.465(7) |
| C(1)–C(2) | 1.506(1) | | |
| Bond Angles (deg) | | | |
| FeO ₆ Octahedron | | | |
| F(1)–Fe–F(3) | 174.6(1) | O(3)–Fe–F(2) | 87.6(2) |
| F(1)–Fe–O(3) | 90.5(2) | O(2)–Fe–F(2) | 174.8(1) |
| F(3)–Fe–O(3) | 90.8(2) | F(1)–Fe–O(1) | 91.7(2) |
| F(1)–Fe–O(2) | 96.5(1) | F(3)–Fe–O(1) | 86.7(2) |
| F(3)–Fe–O(2) | 88.6(1) | O(3)–Fe–O(1) | 175.5(1) |
| O(3)–Fe–O(2) | 92.8(2) | O(2)–Fe–O(1) | 90.9(2) |
| F(1)–Fe–F(2) | 88.7(1) | F(2)–Fe–O(1) | 88.5(2) |
| F(3)–Fe–F(2) | 86.2(1) | | |
| HPO ₃ Tetrahedron | | | |
| O(2) ⁱ –P–O(1) | 114.7(3) | O(2) ⁱ –P–H(1) | 107(2) |
| O(2) ⁱ –P–O(3) ⁱⁱ | 114.3(3) | O(1)–P–H(1) | 107(3) |
| O(1)–P–O(3) ⁱⁱ | 108.6(2) | O(3) ⁱⁱ –P–H(1) | 105(3) |
| (H ₃ N–CH ₂ –CH ₂ –NH ₃) ⁺ /Ethylenediammonium | | | |
| N(1)–C(1)–C(2) | 109.8(3) | N(2)–C(2)–C(1) | 110.6(2) |

^a Symmetry codes: i, $-x + 3/2, -y, z - 1/2$; ii, $x, y, z - 1$.

Magnetic measurements on powdered samples were performed in the temperature range 2.0–300 K, using a Quantum Design MPMS-7 SQUID magnetometer. The magnetic field was 0.1 T, a value in the range of linear dependence of magnetization vs magnetic field, even at 2.0 K.

Results and Discussion

Crystal Structure of $(C_2N_2H_{10})[Fe(HPO_3)F_3]$. The $(C_2N_2H_{10})[Fe(HPO_3)F_3]$ phase exhibits a structure formed by triangular ladder chains extended along the c axis. The $[Fe(HPO_3)F_3]^-$ inorganic framework is constructed of MO_3F_3 isolated octahedra and pseudopyramidal $(HPO_3)^{2-}$ phosphite oxoanions. The ethylenediammonium dications are located in the cavities of the structure delimited by three different chains (Figure 2). The organic dications establish H bonds and ionic interactions with the anionic chains.

The MO_3F_3 octahedra share the trans O(1) and O(3) atoms with the HP(1)O₃ tetrahedra, forming an infinite chain of alternating octahedra and tetrahedra (Figure 3). Each octahedron also shares the O(2) atom from another HP(1)O₃ tetrahedron belonging to a parallel identical chain. An unusual structural feature of this phase is the absence of covalent intrachain $-M-O,F-M-$ bondings, which have been observed in all organically templated phosphite phases with paramagnetic cations.⁶

The Fe^{III} cations of the MO_3F_3 octahedra are bonded to the O(1), O(2), and O(3) atoms of the $(HPO_3)^{2-}$ anions and to the F(1), F(2), and F(3) anions. The mean values of the Fe–O and Fe–F bond distances are 1.98(2) and 1.95(5) Å, respectively. The cis and trans O,F–M–O,F angles range from 86.2(1) to 92.8(2)° and from 174.6(1) to 175.5(1)°,

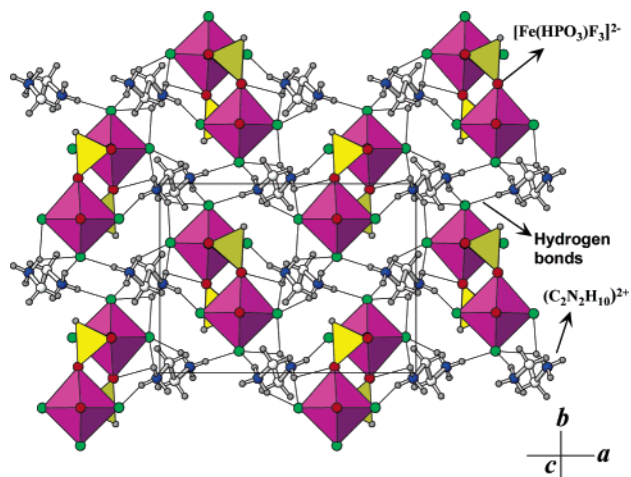


Figure 2. Polyhedral view of the crystal structure of $(C_2N_2H_{10})[Fe(HPO_3)F_3]$ showing the chains along the c axis.

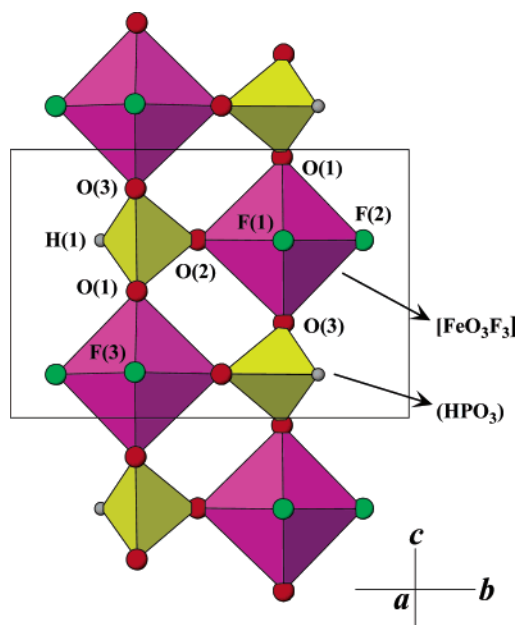


Figure 3. View of the triangular spin ladder chains of $(C_2N_2H_{10})[Fe(HPO_3)F_3]$.

respectively. The $M^{III}-M^{III}$ intermetallic bond distances along the c axis and the triangular pathways are 6.4(1) and 4.9(1) Å, respectively.

In the phosphite anions, the mean value of the P–O bond distances is 1.51(1) Å, with the O–P–O bond angles being those habitually found for a sp^3 tetrahedral hybridization of the central P atom. In this phase, the ethylenediammonium cations establish strong H bonds with the O and F atoms from the inorganic framework. The bond lengths and angles of these H bonds range from 1.80(1) to 2.55(1) Å and from 116.4(1) to 178.6(1)°, respectively (see the Supporting Information).

IR, Raman, UV–Visible, and Mössbauer Spectroscopies. The IR and Raman spectra of $(C_2N_2H_{10})[Fe(HPO_3)F_3]$ exhibit the bands corresponding to the vibrations of the ethylenediammonium dications and the $(HPO_3)^{2-}$ phosphite oxoanions. Selected bands obtained from both the IR and Raman spectra are given in Table 3. It is worth mentioning the

Table 3. Selected Bands (Values in cm^{-1}) for the $(\text{C}_2\text{N}_2\text{H}_{10})[\text{Fe}(\text{HPO}_3)\text{F}_3]$ Phase Obtained from the IR and Raman Spectra^a

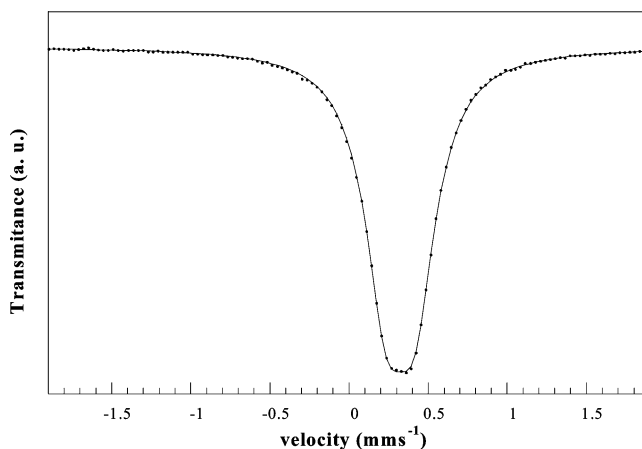
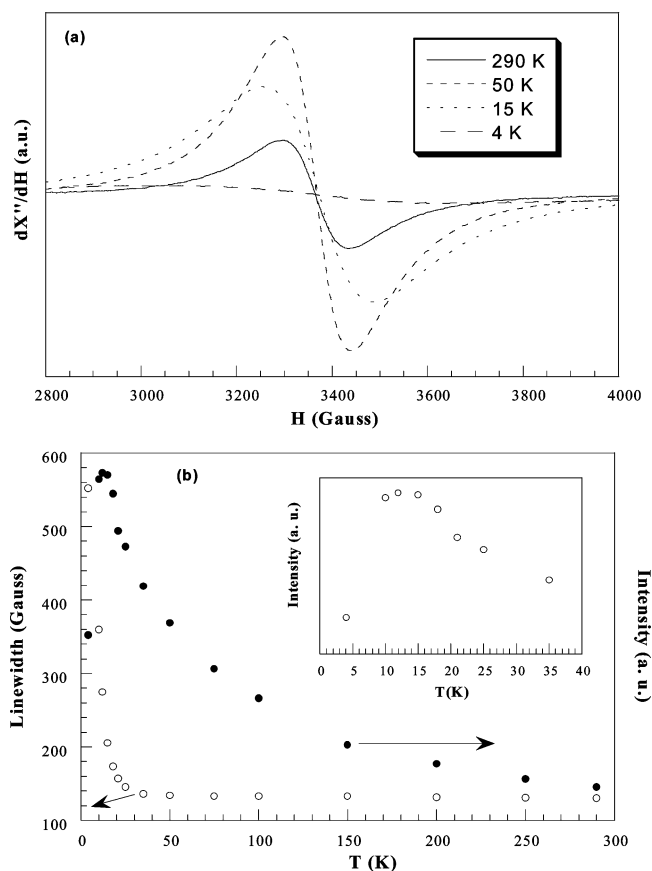
| assignment | IR | Raman |
|-----------------------------------|----------------|----------------|
| $\nu(-\text{NH}_3)^+$ | 3165 (s) | 3015 (w) |
| $\nu(-\text{CH}_2-)$ | 3040 (s) | 2980 (w) |
| $\nu(\text{HP})$ | 2380 (m) | 2380 (s) |
| $\delta(-\text{NH}_3)^+$ | 1615, 1540 (m) | 1615 (w) |
| $\delta(-\text{CH}_2-)$ | | 1460, 1345 (w) |
| $\nu_{\text{as}}(\text{PO}_3)$ | 1085 (s) | 1080 (m) |
| $\nu_{\text{s}}(\text{PO}_3)$ | 1045 (m) | 1060, 1040 (m) |
| $\delta(\text{HP})$ | 1025 (w) | 1030, 1020 (m) |
| $\delta_{\text{s}}(\text{PO}_3)$ | 590 (m) | 580 (w) |
| $\delta_{\text{as}}(\text{PO}_3)$ | 480 (m) | 480 (w) |

^a ν = stretching, δ = deformation, s = symmetric, as = asymmetric, s = strong, m = medium, w = weak.

presence of the vibrational modes of the protonated organic molecule, in good agreement with the structural results. The presence of one band for the $\nu(\text{HP})$ mode of the $(\text{HPO}_3)^{2-}$ oxoanion indicates the existence of only one crystallographically independent phosphite group, in good agreement with the structural results.¹⁴ These data are similar to those found in other related ethylenediammonium compounds.^{6b,e,g,15}

The diffuse-reflectance spectrum shows several weak spin-forbidden transitions in the visible region, which corresponds to a d^5 high-spin cation in an environment with slightly distorted octahedral symmetry. The maxima observed at approximately 14 000, 19 400, 24 800, and 27 600 cm^{-1} have been assigned to the transitions from the ground electronic state ${}^6\text{A}_{1g}({}^6\text{S})$ to the excited-state levels ${}^4\text{T}_{1g}({}^4\text{G})$, ${}^4\text{T}_{2g}({}^4\text{G})$, ${}^4\text{T}_{2g}({}^4\text{D})$, and ${}^4\text{E}_g({}^4\text{D})$, respectively. Taking into account these results, the Dq and Racah (B and C) parameters have been calculated by fitting the experimental frequencies to an energy-level diagram for an octahedral d^5 high-spin system.¹⁶ The values obtained are $Dq = 1030$, $B = 720$, and $C = 3080 \text{ cm}^{-1}$. These values are in the range usually found for octahedrally coordinated Fe^{III} compounds. The reduction of the B-parameter value with respect to that of the free ion (1144 cm^{-1}) is approximately 63%, suggesting a significant covalence in the Fe–O,F chemical bonds.

The Mössbauer spectrum recorded in the paramagnetic state at 300 K is typical of high-spin Fe^{III} ions (Figure 4), indicating nonreduction of this cation during the solvothermal synthesis.¹⁷ The high symmetry exhibited by the FeO_6 octahedron in the crystal structure of this compound determines the existence of a very small splitted doublet, as observed in the Mössbauer spectrum. Taking into account the existence of one crystallographically independent Fe^{III} cation in $(\text{C}_2\text{H}_{10}\text{N}_2)[\text{Fe}_3(\text{HPO}_3)_4]$, the spectrum was fitted to one doublet of Lorentzians using the NORMOS program.¹⁸ The values obtained for the isomer shift and the quadrupole

**Figure 4.** Mössbauer spectrum of $(\text{C}_2\text{N}_2\text{H}_{10})[\text{Fe}(\text{HPO}_3)\text{F}_3]$ at room temperature.**Figure 5.** (a) Powder X-band ESR spectra of $(\text{C}_2\text{N}_2\text{H}_{10})[\text{Fe}(\text{HPO}_3)\text{F}_3]$ at different temperatures. (b) Thermal dependence of the intensity and line width of the signals.

splitting are $0.323\ 90(4)$ and $0.185\ 59(6) \text{ mm s}^{-1}$, respectively, characteristic of Fe^{III} . These values confirm the existence of only one very symmetric crystallographic site for the Fe^{III} cation, as observed from single-crystal X-ray structural refinement.

ESR Spectroscopy. The ESR spectra of $(\text{C}_2\text{N}_2\text{H}_{10})[\text{Fe}(\text{HPO}_3)\text{F}_3]$ were recorded on powdered samples at X band between 4.2 and 300 K. The spectra remain essentially unchanged upon cooling of the sample from room temperature to approximately 50 K. Below this temperature, the signal broadens and the intensity increases. The spectra are

- (14) Nakamoto, K. *Infrared and Raman Spectra of Inorganic and Coordination Compounds*; John-Wiley & Sons: New York, 1977.
- (15) Escobal, J.; Pizarro, J. L.; Mesa, J. L.; Lezama, L.; Olazcuaga, R.; Arriortua, M. I.; Rojo, T. *Chem. Mater.* **2000**, *12*, 376.
- (16) Lever, A. B. P. *Inorganic Electronic Spectroscopy*; Elsevier Science Publisher BV: Amsterdam, The Netherlands, 1984.
- (17) (a) Debord, J. R. D.; Reiff, W. M.; Warren, C. J.; Haushalter, R. C.; Zubietta, J. *Chem. Mater.* **1997**, *9*, 1994. (b) Berrocal, T.; Mesa, J. L.; Pizarro, J. L.; Uriiaga, M. K.; Arriortua, M. I.; Rojo, T. *J. Solid State Chem.* **2006**, in press.
- (18) Brand, R. A.; Larner, J.; Herlach, D. M. *J. Phys.* **1984**, *F14*, 555.

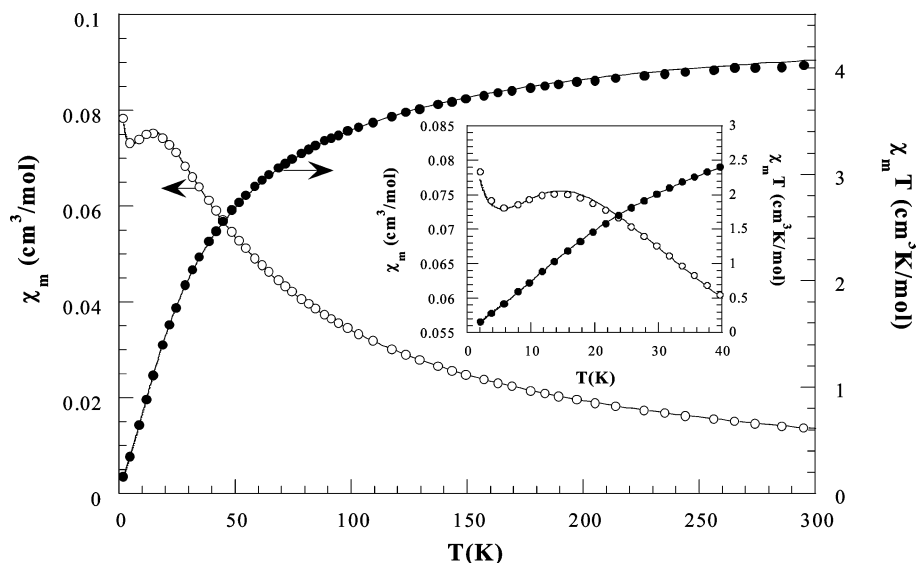


Figure 6. Thermal evolution of the χ_m and $\chi_m T$ curves for Fe^{III} . The solid lines show the best fits.

isotropic with a g value of 2.00(1). This value is characteristic of slightly distorted octahedrally coordinated Fe^{III} ions (Figure 5a).

The temperature dependence of the intensity and line width of the signals calculated by fitting the experimental spectra to Lorentzian curves is displayed in Figure 5b. The intensity of the signal increases with decreasing temperature and shows a maximum at approximately 14 K, after which the intensity decreases again (see the inset in Figure 5b). This result suggests the existence of antiferromagnetic interactions in this compound. The line width of the ESR signals remains practically unchanged from 300 K to approximately 50 K. Below this temperature, the line width increases dramatically because of the existence of a strong spin correlation.¹⁹

The ESR spectra of the Cr^{III} compound were reported in a previous work.^{6g} The spectra show isotropic signals, which correspond to the Cr^{III} cation in a slightly distorted octahedral environment, without variation from room temperature up to 5 K, with a g value of 1.97(1). For the V^{III} phase, only a strong absorption at low magnetic field, characteristic of this cation, was observed.

Magnetic Behavior. The magnetic measurements of the Fe^{III} phase have been performed on powdered samples from room temperature to 2.0 K. Plots of χ_m and $\chi_m T$ curves are shown in Figure 6. The thermal evolution of the χ_m curve follows a Curie–Weiss law at high temperatures ($T > 100$ K), with a Curie constant of 4.38(1) $cm^3 K mol^{-1}$ and a Weiss temperature of $-28.0(1)$ K. The molar magnetic susceptibility increases from room temperature with decreasing temperature and reaches a maximum at approximately 14 K (see the inset in Figure 6). Below this temperature, the magnetic susceptibility decreases, and finally below 6 K, a

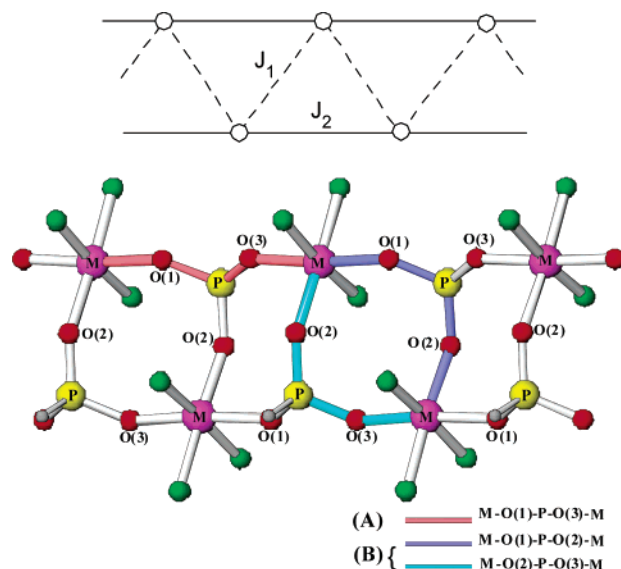


Figure 7. Schematic representation of the possible magnetic-exchange pathways.

weak increase can be observed, probably because of the presence of a paramagnetic impurity. These results together with the continuous decrease in the $\chi_m T$ vs T curve, from 3.99 $cm^3 K mol^{-1}$ at 300 K up to 0.16 $cm^3 K mol^{-1}$ at 2.0 K, indicate that the magnetic interactions in this phase are antiferromagnetic in nature. This result is confirmed by the thermal evolution of the intensity of the signals obtained from the ESR spectra (see Figure 5b).

The data in Figure 6 can be fitted very satisfactorily by using a linear-chain model with second-nearest-neighbor interaction (triangular spin ladder chain; see Figure 7). We can calculate the magnetic susceptibility of this Heisenberg chain by using a closed-chain computational procedure²⁰ as a function of the ratio between both types of interactions, J_1/J_2 , where J_1 is the exchange interaction between first

(19) (a) Wijn, H. W.; Walker, L. R.; Daris, J. L.; Guggenheim, H. *J. Solid State Commun.* **1972**, *11*, 803. (b) Richards, P. M.; Salamon, M. B. *Phys. Rev. B* **1974**, *9*, 32. (c) Escuer, A.; Vicente, R.; Goher, M. A. S.; Mautner, F. *Inorg. Chem.* **1995**, *34*, 5707. (d) Bencini, A.; Gatteschi, D. *EPR of Exchange Coupled Systems*; Springer-Verlag: Berlin/Heidelberg, 1990. (e) Cheung, T. T. P.; Soos, Z. G.; Dietz, R. E.; Merrit, F. R. *Phys. Rev. B* **1978**, *17*, 1266.

(20) Coronado, E.; Drillon, M.; Georges, R. In *Research Frontiers in Magnetochemistry*; O'Connor, C., Ed.; World Scientific Publishing: Singapore, 1993; pp 27–66.

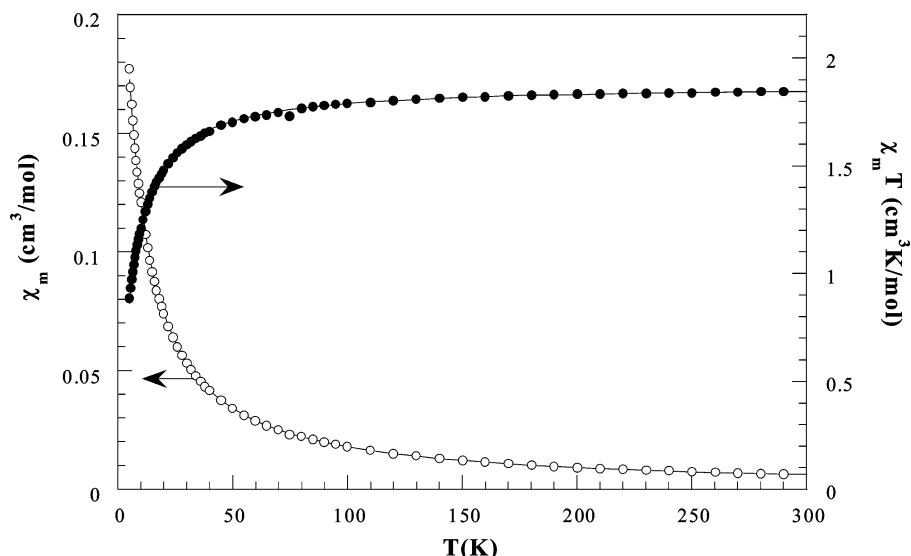


Figure 8. Thermal evolution of the χ_m and $\chi_m T$ curves for Cr^{III} . The solid lines show the best fits.

neighbors and J_2 that between second neighbors. In this procedure, the infinite-chain behavior can be obtained by extrapolation from the exact result for the increasing ring length. The exchange Hamiltonian can be written as

$$\hat{H} = -2J_1 \sum_{i=1}^{N-1} \hat{S}_i \hat{S}_{i+1} - 2J_2 \sum_{i=1}^{N-2} \hat{S}_i \hat{S}_{i+2}$$

where N is the total number of interacting spins. The calculation has been limited up to 8 spins of $S = 5/2$ (135 954 spin states). We have supposed that the $N = 8$ ring is the exact solution in the full experimental temperature range. Calculations were performed with the magnetism package MAGPACK.^{20,21} The best fit from a least-squares analysis of the χ_m vs T curve is $J_1 = -1.63(1)$ K, $J_2 = -0.87(2)$ K, $g = 2.02$ [$g_{\text{ESR}} = 2.00(1)$], and paramagnetic impurity = 1.25% ($R = 6.6 \times 10^{-5}$). The error factor R is defined as $R = \sum(x_{\text{exp}} - x_{\text{calc}})^2 / N x_{\text{exp}}^2$, where N is the number of experimental points.

This model has also been used to fit the magnetic data of the isostructural $(\text{C}_2\text{H}_{10}\text{N}_2)[\text{Cr}(\text{HPO}_3)\text{F}_3]$ compound, which was recently described.^{6g} For this phase, the molar magnetic susceptibility increases with decreasing temperature in the entire temperature range studied (see Figure 8). The thermal evolution of χ_m follows the Curie–Weiss law at temperatures higher than 50 K. The calculated Curie constant and Weiss temperature are $1.88(1) \text{ cm}^3 \text{ K mol}^{-1}$ and $-5.4(1)$ K, respectively.

As can be seen in Figure 8, a constant value of ca. $1.84 \text{ emu K mol}^{-1}$ is obtained for the $\chi_m T$ product at high temperature, which agrees with the presence of one non-interacting Cr^{III} per formula. At temperatures below 100 K, a decrease of $\chi_m T$ appears as a result of the presence of antiferromagnetic interactions. For this Cr^{III} chain, we have applied the same method as that used to fit the magnetic data of the Fe^{III} chain. Again, we can suppose that $N = 8$ is the exact solution. The best fit from a least-squares analysis of the $\chi_m T$ vs T curve (solid line in Figure 8) is $J_1 = -0.56(2)$

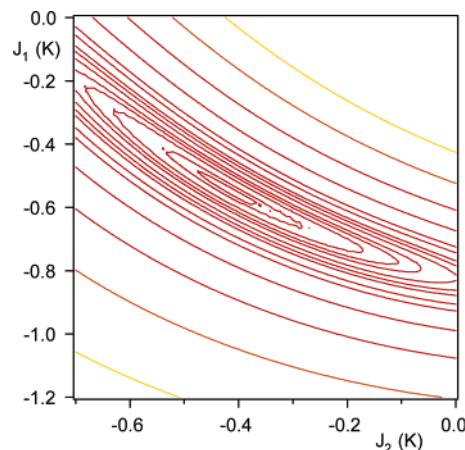


Figure 9. Error contour plot for different J_1 and J_2 values. Calculations were carried out for $g = 2.0$ in the Cr^{III} phase.

$J_1 = -1.63(1)$ K, $J_2 = -0.87(2)$ K, $g = 1.99$ [$g_{\text{ESR}} = 1.97(1)$], and $R = 4.7 \times 10^{-5}$.

To verify the uniqueness of this solution, an exploration of the (J_1, J_2) parameter space was carried out. Figure 9 shows an error contour plot of J_1 vs J_2 for the Cr^{III} phase. The error value is R defined by $R = \sum(xT_{\text{exp}} - xT_{\text{calc}})^2 / N xT_{\text{exp}}^2$. A clear well-defined minimum corresponds to the solution proposed and confirms that the triangular spin ladder chain model is appropriated to the description of the magnetic properties and not a linear-chain model.

The V^{III} compound exhibits a different magnetic behavior, as can be seen in Figure 10. The molar magnetic susceptibility increases with decreasing temperature in the entire temperature range studied. The thermal evolution of χ_m follows the Curie–Weiss law at temperatures higher than 50 K. The calculated Curie constant and Weiss temperature are $0.99(1) \text{ cm}^3 \text{ K mol}^{-1}$ and $-8.1(1)$ K, respectively. The temperature dependence of the $\chi_m T$ product of the V^{III} compound does not have a constant value at high temperatures, and this product decreases continuously from room temperature to 2 K. The best fit obtained with the closed-chain model proposed is $J_1 = -0.85(3)$ K, $J_2 = -1.15(2)$

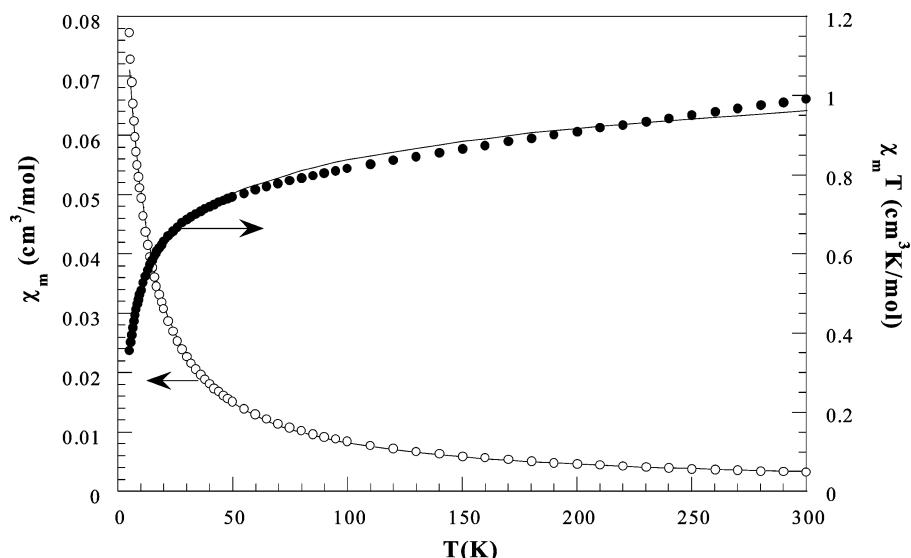


Figure 10. Thermal evolution of the χ_m and $\chi_m T$ curves for V^{III} . The solid lines show the best fits.

Table 4. Bond Angles (deg) and Intermetallic Bond Distances (Å) for the Possible Magnetic-Exchange Pathways in the $(C_2N_2H_{10})[Fe(HPO_3)F_3]$ Compound

| $(enH_2)[Fe(HPO_3)F_3]$ | pathway (a)(b) | Fe–O(a)–P | O(a)–P–O(b) | P–O(b)–Fe | distance Fe–Fe |
|-------------------------|----------------|-----------|-------------|-----------|----------------|
| Fe–O(1)–P–O(3)–Fe | (1)(3) | 141.9 | 108.6 | 143.4 | 6.44 |
| Fe–O(1)–P–O(2)–Fe | (1)(2) | 141.9 | 114.7 | 143.5 | 4.89 |
| Fe–O(2)–P–O(3)–Fe | (2)(3) | 143.5 | 114.3 | 143.4 | 4.89 |
| $(enH_2)[Cr(HPO_3)F_3]$ | pathway (a)(b) | Cr–O(a)–P | O(a)–P–O(b) | P–O(b)–Cr | distance Cr–Cr |
| Cr–O(1)–P–O(3)–Cr | (1)(3) | 145.3 | 110.6 | 140.9 | 6.51 |
| Cr–O(1)–P–O(2)–Cr | (1)(2) | 145.3 | 115.2 | 141.4 | 4.88 |
| Cr–O(2)–P–O(3)–Cr | (2)(3) | 141.4 | 113.4 | 140.9 | 4.88 |
| $(enH_2)[V(HPO_3)F_3]$ | pathway (a)(b) | V–O(a)–P | O(a)–P–O(b) | P–O(b)–V | distance V–V |
| V–O(1)–P–O(3)–V | (1)(3) | 141.9 | 108.5 | 142.0 | 6.44 |
| V–O(1)–P–O(2)–V | (1)(2) | 141.9 | 115.4 | 141.7 | 4.89 |
| V–O(2)–P–O(3)–V | (2)(3) | 141.7 | 114.9 | 142.0 | 4.89 |

K , $g = 1.80$, and $TIP = 5.9 \times 10^{-4}$ ($R = 8.1 \times 10^{-4}$). However, the quality of the fit is not the same as that for Fe^{III} and Cr^{III} phases. The origin of this difference can be attributed to the existence of a big anisotropy for the V^{III} phases as much in the g factor as in the presence of a zero-field-splitting parameter, D , as was observed from the ESR data. In addition, we can expect that D can be bigger than the exchange interactions. The continuous drop in the $\chi_m T$ product has its origin in both the anisotropy and antiferromagnetic exchange. In this case, the triangular spin ladder chain model did not work. However, another fit considering only a linear chain and a D value for each center gives a solution of worse quality, but it can help us to estimate a D value of around 2.5 cm^{-1} and an average exchange parameter of $-1.15(1) \text{ K}$. The value of the D parameter is similar to those observed in other V^{III} phases.²²

Taking into account the structural features of these compounds (see Figure 7), the following can be observed:

- (21) (a) Borrás-Almenar, J. J.; Clemente-Juan, J. M.; Coronado, E.; Tsukerblat, B. S. *Inorg. Chem.* **1999**, *38*, 6081. (b) Borrás-Almenar, J. J.; Clemente-Juan, J. M.; Coronado, E.; Tsukerblat, B. S. *J. Comput. Chem.* **2001**, *22*, 985.
- (22) (a) Rojo, J. M.; Mesa, J. L.; Calvo, R.; Lezama, L.; Olazcuaga, R.; Rojo, T. *J. Mater. Chem.* **1998**, *8* (6), 1423. (b) Bencini, A.; Gatteschi, D. *EPR of Exchange Coupled Systems*; Springer-Verlag: Berlin/Heidelberg, 1990.

(i) The M–O(1)–P–O(3)–M lineal pathway links the M^{III} cations along the triangular ladder chain through one $(HPO_3)^{2-}$ phosphite anion. The distances $M \cdots M$ are approximately 6.44, 6.51, and 6.44 Å for Fe^{III} , Cr^{III} , and V^{III} , respectively. (ii) The M–O(1)–P–O(2)–M and M–O(2)–P–O(3)–M transversal pathways connect the metallic centers placed in every chain belonging to the triangular ladder chain, with $M \cdots M$ intermetallic distances of approximately 4.89, 4.88, and 4.89 Å, respectively. The deviation of the bond angles from the value of 90° , shown in Table 4, suggests that the mean magnetic interactions should be antiferromagnetic,²³ in good agreement with the results obtained from the magnetic fits of the experimental data. Furthermore, these super-superexchange pathways via phosphite oxoanions should give weak magnetic couplings, as was obtained from the magnetic fits.

Concluding Remarks

A new organically templated material based on the Fe^{III} cations and the $(HPO_3)^{2-}$ phosphite oxoanions has been prepared under solvothermal conditions in the form of single crystals. The crystal structure shows the existence of

- (23) Goodenough, J. B. *Magnetism and the Chemical Bond*; Interscience: New York, 1963.

triangular spin ladder chains, without M–O,F–M covalent bondings. The calcination of the ethylenediammonium dications originates the collapse of the structure. The IR spectroscopy corroborates the presence of one crystallographically independent phosphite oxoanion and the presence of protonated organic groups. The spectroscopic data in the visible region allowed us to calculate the Dq and Racah parameters, which are in the range habitually found for the Fe^{III} cations in slightly distorted octahedral geometry. Mössbauer spectroscopy confirms the existence of very symmetrical octahedral Fe^{III} cations. From the thermal evolution of the ESR signals and the magnetic data, the presence of antiferromagnetic interactions can be proposed for this new Fe^{III} phosphite compound. The *J*-exchange parameters for the (C₂H₁₀N₂)[M(HPO₃)F₃] compounds, M^{III} = Fe, Cr, and V, have been calculated by fitting the experimental magnetic data as a function of the ratio between both types of interactions, *J*₁/*J*₂, where *J*₁ represents the magnetic interaction between first neighbors and *J*₂ that between second neighbors. The fits give a good solution for the Fe^{III} and Cr^{III} compounds. However, the V^{III} phase has a different magnetic behavior because of its big anisotropy and the

existence of a zero-field-splitting parameter. In this case, a fit with only a linear chain and a *D* value for each center allowed us to estimate values of *D* = 2.5 cm⁻¹ and *J* = -1.15(1) K.

Acknowledgment. This work has been financially supported by the “Ministerio de Educación y Ciencia” (MAT-2004-02071) and the Universidad del País Vasco (UPV/EHU; 9/UPV00130.310-15967/2004 and 9/UPV00169.310-13494/2001). The authors thank the technicians of S. G. Iker and Dr. J. P. Chapman, financed by the “National Program for the Promotion of Human Resources within the National Plan of Scientific Research, Development and Innovation—“Ministerio de Ciencia y Tecnología” and “Fondo Social Europeo”, for the X-ray diffraction and magnetic measurements, respectively. S.F.-A. thanks the Gobierno Vasco/Eusko Jaurlaritza for funding.

Supporting Information Available: Crystallographic data (CIF file). This material is available free of charge via the Internet at <http://pubs.acs.org>. This material can also be obtained free of charge from the Cambridge Crystallographic Data Centre (CCDC 224863). IC051804O